Modulation of the Optical Response of Polyethylene Films Containing Luminescent Perylene Chromophores

Filippo Donati,[†] Andrea Pucci,*[,†] Chiara Cappelli,[†,‡] Benedetta Mennucci,[†] and Giacomo Ruggeri[†,‡,§]

Dipartimento di Chimica e Chimica Industriale, and PolyLab-CNR, c/o Dipartimento di Chimica e Chimica Industriale, Università di Pisa, Via Risorgimento 35, I-56126 Pisa, Italy, and INSTM, Unità di Ricerca di Pisa, Via Risorgimento 35, I-56126 Pisa, Italy

Received: November 26, 2007; In Final Form: January 8, 2008

In this work, two perylene derivatives containing different peripheral alkyl chains (i.e., *N*,*N*′-bis-(hexyl)-perylene-3,4,9,10-tetracarboxyldiimide (ES-PTCDI) and *N*,*N*′-bis-(2′-ethylhexyl)perylene-3,4,9,10-tetracarboxyldiimide (EE-PTCDI)) were synthesized and efficiently dispersed at low loadings (from 0.01 to 0.1 wt %) into linear low-density polyethylene (LLDPE) by processing in the melt. Spectroscopic investigations (UV−vis and fluorescence) combined with quantum-mechanical studies demonstrated the ability of both chromophores to generate aggregates among the planar structure of dyes when dissolved in solution or dispersed into LLDPE above a certain concentration. The data acquired for dyes' dispersions into the polymer matrix reveal that the optical properties and responsiveness to mechanical stimuli are strongly dependent on the compactness of perylene aggregates provided by the different molecular structure of dyes. In particular, the strong intermolecular aggregates of ES-PTCDI resulted in being more resistant toward mechanical stress and less orientable by uniaxial drawing along the drawing direction of the film, whereas the less compact and distorted supramolecular architecture of EE-PTCDI chromophores provided composite films with a remarkable optical response to mechanical solicitations.

Introduction

In recent years, the research of new, easy, and effective methods for the determination of external contaminations of plastic packages has grown greatly. For example, highly sensitive optical techniques based on the luminescence of conjugated aromatic molecular additives dispersed at low concentrations (less than 1−2 wt %) into the amorphous phase of thermoplastic polymers were successfully applied to the detection of thermal and mechanical solicitations on plastic films.[1−12] The luminescent dyes incorporated into polymers as thermodynamically stable micro-/nano-sized aggregates of a few molecules show emission characteristics coming mostly from the fluorescence of interacting chromophores through $\pi-\pi$ stacking interactions among the planar aromatic backbones. On applying a mechanical deformation to the polymeric film, the shear-induced mixing between the continuous macromolecular matrix and the additive phase promoted the break-up of dye aggregates and the prevalence of the emission coming from isolated non-interacting chromophores, leading to a clear change in the material's emission properties.[2,11] On the contrary, polymeric films optically sensitive to thermal solicitations are generally prepared by the incorporation of kinetically trapped luminescent dyes. In such a situation, the dyes are frozen in a non-interacting supramolecular fashion but easily are perturbable by a thermal solicitation above a certain temperature (strictly depending on the nature of the polymer matrix) that induces the formation of thermodynamically stable chromophoric aggregates.[1,3,7] As luminescent additives incorporated into polymers for sensing applications, oligo(*p*-phenylene vinylene) and stilbene derivatives were the most exploited due to their fluorescence response that was highly dependent on the chromophore aggregation extent. Among this class of dyes, considerable attention recently has been devoted in the literature to perylene based chromophores, due to the effective combination of properties ranging from electro-optical and redox characteristics to thermal and migration stability.[13,14] Perylene molecules consist of planar five benzene rings fused together, whose structure and electronic conformation strongly promote the formation of chromophoric aggregates through stacking interactions between the conjugated cores. An interesting exhaustive review focused on the supramolecular organization of perylene derivatives to form complex functional architectures recently has been proposed by Würthner.[15] The self-organization of functional perylenes was reported as being fundamental to tailor defined multi-chromophoric materials with a modulable optoelectronic response.

Perylene derivatives are nowadays employed for various optoelectronic applications, thanks to their thermal and photostability, as, for example, fluorescence standards, thin film transistors, liquid crystals, light emitting diodes, and devices for photovoltaics.[16−20] In addition, according to the first work reported by Langhals et al.[16] and profiting from the versatility and reactivity of the perylene tetracarboxylic acid bis-anhydride, perylene dyes are often peripherally functionalized by a multitude of aromatic and/or aliphatic moieties to enhance their

* Corresponding author. Tel.: +39 050 2219270; fax: +39 050 2219320; e-mail: apucci@ns.dcci.unipi.it.
† Dipartimento di Chimica e Chimica Industriale, Università di Pisa.
‡ PolyLab-CNR, c/o Dipartimento di Chimica e Chimica Industriale, Università di Pisa.
§ INSTM, Unità di Ricerca di Pisa.

10.1021/jp711193u CCC: $40.75
Published on Web 03/05/2008

optoelectronic properties or to strongly increase their solubility into several dispersing media.[15,16,21,22]

Intrigued by the possibility of generating multi-chromophoric supramolecular architectures even when dispersed into a semicrystalline polymer matrix, we report in this work the use of perylene derivatives as innovative luminescent probes for plastic films. In particular, two perylene tetracarboxylic acid bis-imides (perylene bis-imides) (i.e., *N*,*N*′-bis-(hexyl)perylene-3,4,9,10-tetracarboxyldiimide (ES-PTCDI) and *N*,*N*′-bis-(2′-ethylhexyl)-perylene-3,4,9,10-tetracarboxyldiimide (EE-PTCDI)) were synthesized by symmetric peripheral functionalization through a condensation reaction of perylene tetracarboxylic acid bis-anhydride with the linear hexylamine or the branched 2-ethyl-hexylamine, respectively. The optical properties of the dyes were first characterized in solution, focusing the attention to their aggregation behavior in different classes of solvents. Quantum-mechanical calculations were used to obtain better insight into the nature of absorbing and emitting states both as a single molecule (possibly with the inclusion of solvent effects) and as dimeric aggregates.

The dyes were also dispersed by melt processing into a polyolefinic thermoplastic matrix (i.e., linear low-density polyethylene (LLDPE)) at different concentrations. All the films prepared were studied in terms of their absorption and emission behavior as a function of the type of molecule, concentration, and polymer drawing extent, and the results were compared with calculations and discussed in terms of their use as highly sensitive polyethylene indicators to mechanical solicitations.

Experimental Procedures

Materials. LLDPE (Dowlex SC 2107, melt flow index, 190 °C/2.16 kg/ 2.3 g/10 min, $d = 0.917$ g/cm^3, supplied by Dow Plastics) was used as the polymer host matrix.

Perylene-3,4,9,10-tetracarboxydianhydride (PTCDA), imidazole, hexylamine, and 2-ethyl-hexylamine were supplied by Aldrich and used without further purification.

Samples were named by listing the guest molecule (abbreviated as ES or EE), polymer (abbreviated as LLDPE), and concentration (e.g., EE-LLDPE-0.02).

Apparatus and Methods. ^{1}H− and ^{13}C NMR spectra were recorded with the help of a Varian Gemini 200 MHz instrument using 5−10% $CDCl_3$ (Aldrich, 99.8 atom % D) solutions. NMR spectra were registered at 20 °C, and the chemical shifts were assigned in ppm using the solvent signal as a reference. FT-IR spectra were recorded with the help of a PerkinElmer Spectrum One spectrometer on dispersions in KBr. Elementary analyses were obtained by the microanalysis laboratory in the Faculty of Pharmacy, University of Pisa. Thermogravimetric scans were obtained by means of a Mettler-Toledo Star-system TGA-SDTA-851 under nitrogen flux, at a scan rate of 20 °C/min. LLDPE blends were prepared in a Brabender plastograph mixer (model OHG47055, 30 cm^3) under nitrogen atmosphere by introducing approximately 20 g of the polymer and 0.01−0.1 wt % dye in the mixer at 180 °C with a rotor speed of 50 rpm. After 10 min, the mixing was stopped, and the recovered materials were ground at room temperature by using an IKA MF10 analytical mill. The powder obtained was successively molded between two pieces of aluminum foil under compression in a Collin model 200M press at 180 °C for 5 min.

After removal from the press, the films were allowed to reach room temperature slowly (∼ 5 °C min^{-1}). The films were generally analyzed after 2−3 days. The thickness of the obtained films was in the range of 80−150 μm. Optical absorption studies of $CHCl_3$ and *n*-heptane solutions (10^{-4} to 10^{-6} M) and polymer films were carried out at room temperature with the help of a Perkin−Elmer Lambda 650 equipped with motor-driven Glan-Taylor linear polarizers. Steady-state fluorescence spectra of solutions and polymer films were acquired under isotropic excitation with the help of a PerkinElmer luminescence spectrometer LS55 controlled by FL Winlab software and equipped with the front surface accessory. Solid-state drawings of the binary films were performed at room temperature or at 90 °C on a thermostatically controlled hot stage. The draw ratio (Dr), defined as the ratio between the final and the initial length of the sample, respectively, was determined by measuring the displacement of ink-marks printed onto the films before stretching. The scanning electron microscopy (SEM) analysis was performed with a Jeol 5600-LV microscope, equipped with an Oxford X-ray EDS microprobe, an instrument at the chemical engineering department of the University of Pisa. The absorption anisotropies were quantitatively evaluated by calculating the dichroic ratio R (defined as $R = A_{//}/A_{\perp}$) of the absorption intensities (A).[12] The films' roughness was diminished, using ultrapure silicon oil (poly(methyl phenylsiloxane), 710 fluid, Aldrich) to reduce surface scattering between the polymeric films and the Suprasil quartz slides, used to keep them planar. In the analysis of the absorption and emission data, the scattering contribution was corrected by the use of appropriate baselines. Origin 7.5, software by Microcal Origin, was used in the analysis of the absorption and emission data.

Synthesis of ES-PTCDI. A total of 0.45 g (1.14 mmol) of PTCDA was dissolved in 9.20 g of imidazole at 90 °C. Then, 0.36 mL (2.76 mmol) of hexylamine was added to the solution, and the mixture was warmed to 180 °C and stirred for 4 h. After cooling to room temperature, the solution was treated with 10 mL of water and then with 70 mL of 2 N HCl. The mixture was stirred for 12 h, and the resulting dark-red solid was filtered off and washed thoroughly with distilled water until the pH of the washings turned to be neutral and dried. The crude product was purified by chromatography on silica gel using chloroform/ethyl acetate 20:1 by volume as the eluent: 0.455 g (0.82 mmol, yield: 71.5%) of a deep-red solid was recovered. IR (KBr): 3093 (υCH arom), 2952, 2948, 2857 (υCH aliph), 1695, 1653, 1594 (υCO imide), 1504, 1440, 1398, 1342 (υCC ring) cm^{-1}. ^{1}H NMR: 8.6 (d, 4H arom, $J = 7.97$ Hz), 8,5 (d, 4H arom, $J = 7.91$ Hz), 4,1 (t, 4H, N-CH_2, $J = 7.45$ Hz), 1,3 (m, 16H + 6H, -CH_2-, -CH_3) ppm. ^{13}C NMR: 162 (CO), 137, 131, 129, 122 (CC arom) ppm. ($C_{49}H_{34}N_2$) (650): calcd C 77.4, H 6.0, N 5.0; found C 77.3, H 5.9, N 4.8. UV−vis ($CHCl_3$): $\lambda_{max} = 520$ nm ($\epsilon_{520} = 49\,000$ L cm^{-1} mol^{-1}). Emission ($CHCl_3$, $\lambda_{exc} = 280$ nm): $\lambda_{emmax} = 543$ nm.

Synthesis of EE-PTCDI. This compound was prepared following the procedure outlined for the synthesis of ES-PTCDI but substituting hexylamine with 2-ethyl-hexylamine (0.44 mL, 2.76 mmol). A total of 0.580 g (0.94 mmol, yield: 82.8%) of a deep-red solid was recovered. IR (KBr): 3093 (υCH arom), 2952, 2948, 2857 (υCH aliph), 1695, 1653, 1594 (υCO imide), 1577, 1504, 1440, 1398, 1342 (υCC ring) cm^{-1}. ^{1}H NMR: 8.5 (d, 4H arom, $J = 7.97$ Hz), 8.3 (d, 4H arom, $J = 8.10$ Hz), 4.1 (m, 4H, N-CH_2), 1.9 (m, 2H, CH) 1.3 (m, 16H, CH_2), 0.9 (m, 12H, CH_3) ppm. ^{13}C NMR: 163 (CO), 136, 131, 128, 122 (CC arom) ppm. ($C_{50}H_{42}N_2$) (670.0): calcd C 77.28, H 7.11, N 4.74; found C 77.00, H 7.17, N 4.50. UV−vis ($CHCl_3$): $\lambda_{max} = 523$ nm ($\epsilon_{523} = 78\,800$ L cm^{-1} mol^{-1}). Fluorescence ($CHCl_3$, $\lambda_{exc} = 238$ nm): $\lambda_{emmax} = 537$ nm.

Computational Details. In all calculations, a model PTCDI system was used in which side groups were replaced by methyl groups; from now on, this system will be indicated as Me-

SCHEME 1: Synthetic Path Followed in Perylene Dye Preparation

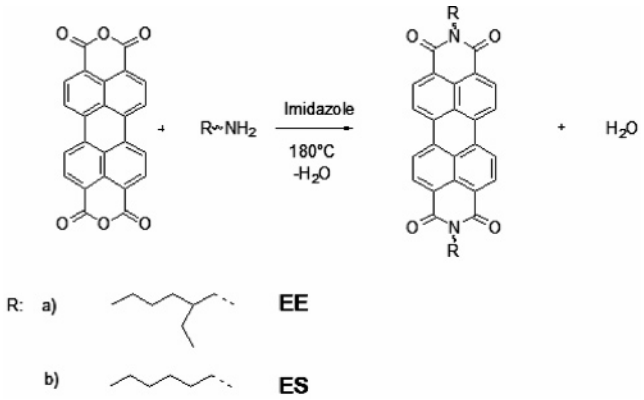

PTCDI. Ground-state and first excited-state geometries were obtained using Hartree−Fock (HF) calculations and density functional theory (DFT) and configuration interaction singles (CIS) and time-dependent DFT (TDDFT), respectively. All DFT calculations were performed using the B3LYP hybrid functional.[23,24] In all cases, the 6-31+G(d) basis set was exploited. Absorption and emission energies were calculated at the CIS, TDDFT, and ZINDO levels, in the last case with CIS geometries. Solvent effects were taken into account using the polarizable continuum model (PCM):[25] within this framework, the solute is described as a quantum-mechanical charge distribution embedded in a cavity inside a dielectric continuum. The shape and size of the cavity are defined according to the solute geometry using an envelope of interlocking spheres centered on selected atoms (here, all C, N, and O atoms). In the PCM method, the effects of the solute−solvent mutual polarization are accounted for in all steps of the calculation. This was obtained using a quantum-mechanical framework in which the solvent reaction potential contributes to the system Hamiltonian. All calculations were performed using the Gaussian (G03) computational code.[26]

Results and Discussion

With the aim to achieve optically responsive films toward external stimuli, two perylene bis-imide derivatives symmetrically functionalized by linear or branched alkyl chains were synthesized and successively dispersed at low concentrations (less than 0.1 wt %) into LLDPE.

First, the two different perylene based chromophores (ES-PTCDI and EE-PTCDI) were prepared by the condensation of perylene tetracarboxylic acid bis-anhydride with two different aliphatic amines, to confer on the dye a good compatibility toward the apolar polymer matrix (Scheme 1).[9,12,27]

Both perylene dyes were obtained in good yields (71.5% for ES-PTCDI and 82.8% for EE-PTCDI) as dark-red solids very soluble in chlorinated solvents. They showed high melting points (higher than 300 °C) and degradation temperatures of 474 °C (EE-PTCDI) and 448 °C (ES-PTCDI), as measured by thermogravimetric analysis (TGA) in air.

Optical Characterization in Solution. As reported by Langhals et al. and Würthner,[15,28] perylene dyes obtained according to the approach reported in Scheme 1 were characterized by the same absorption and emission features due to the presence of nodes in the HOMO and LUMO at the imide nitrogen, which avoided the electronic coupling between the perylene nuclei and the imide substituents. For example, EE-PTCDI dissolved in $CHCl_3$ showed three pronounced absorption peaks (in the range of 450−550 nm) and a shoulder at around 425 nm, which correspond, respectively, to the 0−0, 0−1, 0−2, and 0−3 vibronic transitions.[29] The plot of the absorption maximum of EE-PTCDI at 524 nm as a function of molar concentration showed typical linear Lambert−Beer behavior (Figure 1a). The fluorescence spectra reported in Figure 1b depicted the same peak structure in a mirror image of the absorption with emission maxima at about 530 and 575 nm. In particular, the red-shift of the 0−0 radiative transition band of about 10 nm (from 534 to 543 nm) that occurred with increasing the EE-PTCDI concentration, flanked by the decrease of the ratio between the intensity of 0−0 and the intensity of 0−1 relaxations, was attributed to self-absorption phenomena.[30]

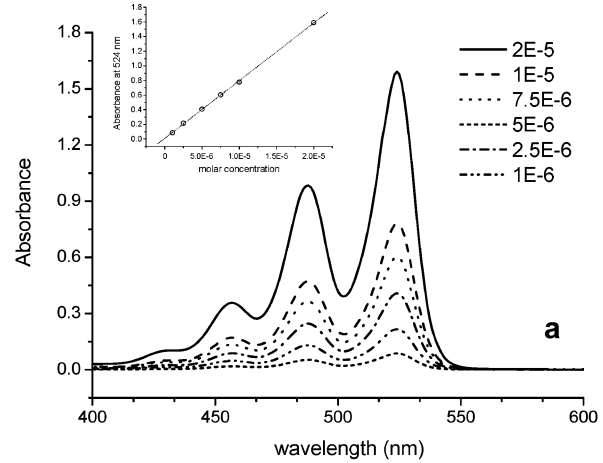

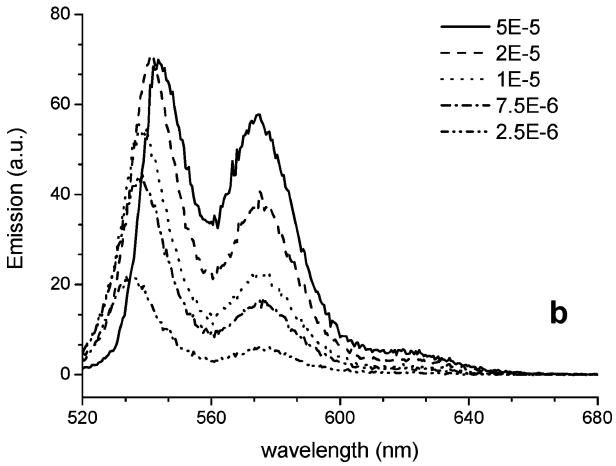

Figure 1. (a) UV−vis absorption and (b) fluorescence spectra (λ_{exc} = 280 nm) of EE-PTCDI in $CHCl_3$ at different concentrations and dependence of absorption maxima at 524 nm with dye concentration (inset of panel a).

In both absorption and emission spectra, no bands attributed to the formation of chromophoric aggregates were detected in the range of concentrations investigated (10^{-6} to 2×10^{-5}). The same behavior (data not reported) was obtained for the analogue ES-PTCDI dye dissolved in $CHCl_3$.

On the contrary, when ES-PTCDI and EE-PTCDI were dispersed into a completely apolar and non-interacting solvent such as heptane, the absorption and emission features strongly changed upon increasing the concentration. This behavior is in accordance with what has been reported previously in the literature.[29] As reported in Figure 2a for EE-PTCDI in heptane, a new absorption band emerged at about 560 nm flanked by a progressive loss of the vibronic fine structure of the higher

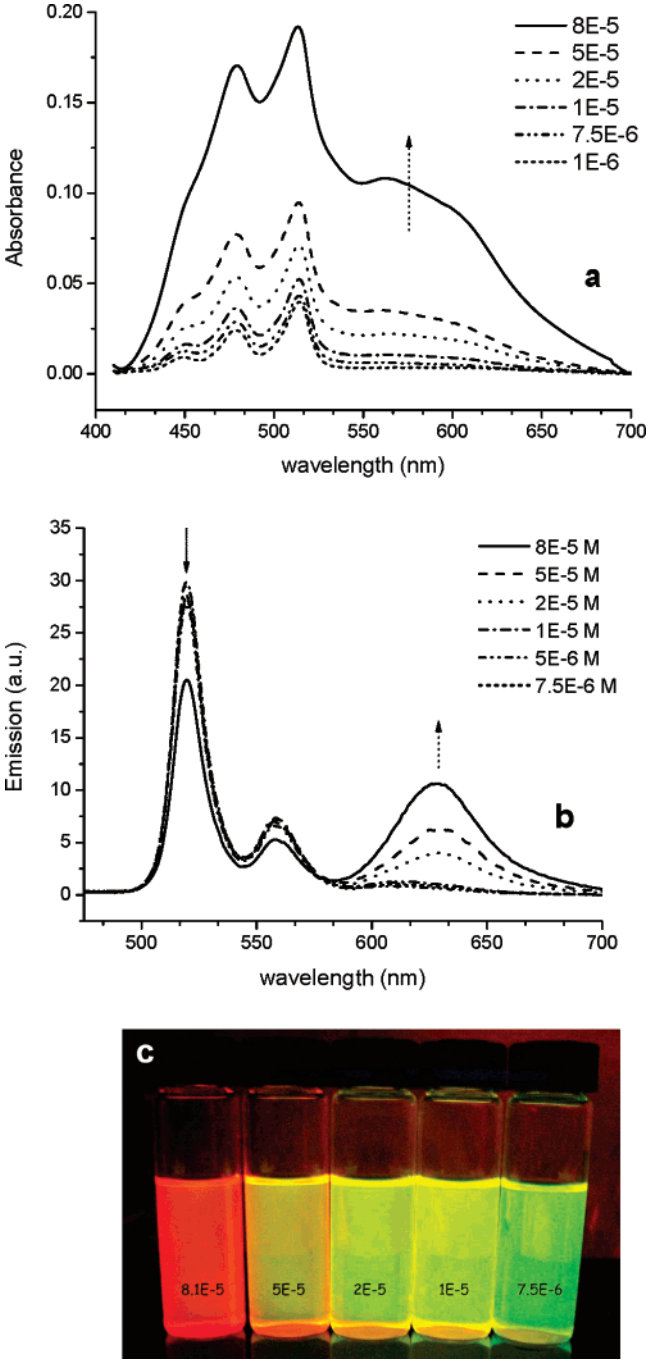

Figure 2. (a) UV−vis absorption and (b) fluorescence spectra (λ_{exc} = 300 nm) of EE-PTCDI in heptane at different concentrations and (c) image of the same dispersions taken under irradiation at 366 nm.

energy 0−1 and 0−2 transitions (at approximately 480 and 450 nm, respectively), suggesting the formation of molecular dye aggregates likely caused by effective $\pi-\pi$ stacking co-facial interactions among perylene nuclei.[29]

Analogous to the absorption, the emission behavior of the heptane dispersions (Figure 2b) depicted the typical formation of luminescent aggregates. A new band actually emerged at higher wavelengths at about 630 nm, the intensity of which tended to overcome the main emission attributed to the luminescence of isolated EE-PTCDI chromophores at 525 nm.[31] In particular, the partial quenching of the band at 525 nm that occurred with increasing concentration was attributed to the electronic coupling between perylene chromophores as well. Interestingly, the occurrence of supramolecular chromophore

TABLE 1: Calculated Absorption Energies (λ) and Oscillatory Strengths (f) of Me-PTCDI Obtained at Various Levels of Theory in Different Solvents[a]

	VAC		$CHCl_3$		DMSO	
	λ (nm)	f	λ (nm)	f	λ (nm)	f
ZINDO	482	1.184	529	1.321	539	1.352
CIS	389	1.190	408	1.346	409	1.366
TDB3LYP	533	0.682	563	0.879	567	0.898
EXP	(479−515)[b]		(488−525)			

[a] Experimental values refer to ES-PTCDI. [b] Measured in *n*-heptane.

TABLE 2: Calculated Emission Wavelengths (λ) and Oscillatory Strengths (f) of Me-PTCDI Obtained at Various Levels of Theory[a]

	λ (nm)	f
ZINDO	521	1.1514
CIS	426	1.1482
TDB3LYP	577	0.651
EXP	525	

[a] Experimental value refers to ES-PTCDI in *n*-heptane.

interactions among perylene derivatives in heptane dispersions was visually detected by exciting the samples with a long-range UV lamp at 366 nm. The color of the liquids changed from yellow−green (associated with non-interacting perylene dyes) to red (associated with perylene aggregates) with a change in concentration (Figure 2c).

To gain more detailed information at the molecular level, the experimental absorption and emission energies were compared with quantum-mechanical (QM) calculations using different descriptions for both isolated and solvated model Me-PTDI systems (see Computational Details).

In Table 1, absorption energies and oscillatory strengths of the model Me-PTCDI in the gas phase and $CHCl_3$ and DMSO solutions together with experimental values measured for EE-PTCDI in *n*-heptane and $CHCl_3$ solutions at low concentrations are reported.

At all levels of calculations and in all different environments, the nature of the absorbing state remains constant, and it can be described as a $\pi-\pi^*$ excitation with a dominant contribution from the HOMO−LUMO transition, as expected. Such a transition is characterized by a significant dipole moment directed along the main axis of the molecule.

Moving to the comparison with experiments, the best agreement is obtained at ZINDO both in the gas phase and in solution, whereas CIS wavelengths are always too small and TDB3LYP ones too large: this behavior is not unexpected as CIS is well-known to overestimate excitation energies. The observed solvatochromic (red) shift moving from apolar *n*-heptane to $CHCl_3$ is correctly reproduced by calculations (notice that in the calculations, we have assumed *n*-heptane to be approximated by vacuum). A very small change is found when moving from $CHCl_3$ to the more polar DMSO, thus showing that this excitation is almost insensitive to polarity effects.

Because of this low sensitivity to the solvent of the excitation process, we limited the computational analysis of the emission to the isolated system only. In Table 2, the results obtained at the three different levels are reported, together with the experimental values measured for EE-PTCDI in *n*-heptane at low concentrations. In all cases, a CIS optimized geometry of the excited state was used. As can be seen from the comparison with the experimental emission wavelength, once again, the ZINDO level gives the best description.

SCHEME 2: Model of Transition Dipole Interactions in Dye H- and J-Aggregates and Resulting Absorption Properties

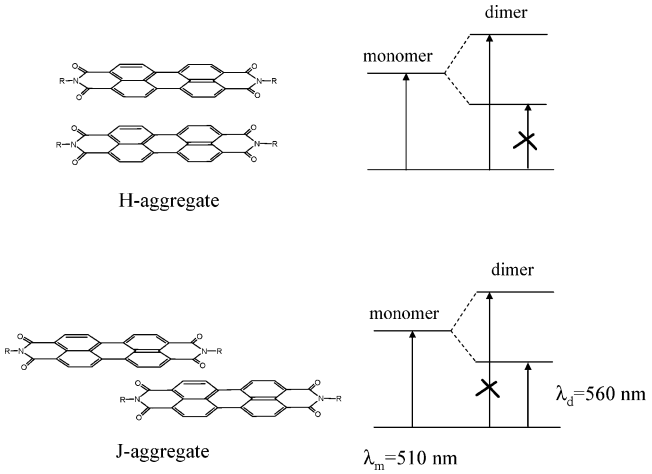

Starting from the good results obtained at the ZINDO level for both absorption and emission of Me-PTCDI, in the following discussion, we will attempt to characterize the aggregates giving rise to the red-shifted band appearing in the absorption and emission spectra of EE-PTCDI at high concentrations (see Figure 2).

By assuming the exciton theory to be valid, such a new band can be explained as the result of the coupling between the two transition densities of the monomer when forming a dimer aggregate. According to this theory, the position of the dimer band with respect to that of the monomer depends on the mutual position of the two interacting monomers. In Scheme 2, a graphical representation of what should be observed for H- and J-type aggregates is reported.

From our experimental data (also shown in the picture), it emerged that H-type aggregates actually were not present in our systems. Following this, different J-type aggregates were explored, as obtained by changing the internuclear distance and the tilt angle (i.e., the angle that distinguishes H- from J-type aggregates).

To confirm the prediction reported previously, absorption and emission energies of model dimer systems were calculated; dimers were obtained by assuming that the structure of each monomer remained fixed when a dimer was formed. Also, only longitudinal shifts (along the monomer main axis) and not transverse shifts (along the short axis) or rotation were assumed.

Three different stacking distances were considered (i.e., $R_1 = 3.33$, $R_2 = 3.43$, and $R_3 = 3.53$ Å), which typically are observed in the crystal structures of these systems,[15] and the longitudinal shift (i.e., the distance between the center of a monomer and the center of the second monomer projected on the first) ranged from 0 (i.e., tilt angle $\alpha = 90°$) to 14 Å (i.e., tilt angle $\alpha = 15°$). All the calculations were performed at the ZINDO level by using an optimized monomer B3LYP/6-31+G(d) ground-state structure and an optimized monomer CIS/6-31+G(d) excited-state structure. Transition energies for both absorption and emission are reported in Figure 3 as a function of the α tilt angle.

As can be seen from Figure 3, calculations indicate that there exists a window of values ($65° < \alpha < 45°$) in which the expected red-shift is observed (a similar window is found for both absorption and emission). The magnitude of the shift obviously depends on the stacking distances, the maximum value being found at the shortest distance ($R_1 = 3.33$ Å) at which the wavelength is 540 nm for absorption and 585 nm for emission. These values have to be compared with the measured maxima of 560 nm for absorption and 620 nm for emission. Combining these values with those reported in Tables 1− and 2, and converting them into energies, it results that the calculated red-shift is slightly overestimated for absorption (0.28 eV vs 0.20 eV) and underestimated for emission (0.26 eV vs 0.36 eV).

To be more quantitative, possible transversal shifts (t) were considered because they are generally found in crystal structures: the measured transversal shifts generally range between 0.5 and 1.5 Å, depending on the terminal group.[32−36] In this analysis, only a single tilt angle ($\alpha = 50°$) and the two shortest distances ($R_1 = 3.33$ and $R_2 = 3.43$ Å) were considered. The results are reported in Figure 4.

As it can be seen from Figure 4, by increasing the transversal, a smaller red-shift with respect to the monomer is predicted, both in absorption and in emission; for large t values (>1 Å), a blue-shift is predicted. This behavior can be related to a decreasing interaction between the two monomers when t increases.

Optical Properties of LLDPE Based Films. *Effect of Dye Concentration.* The 80−150 μm thick LLDPE films containing different concentrations of ES-PTCDI or EE-PTCDI (0.01−0.1 wt % dye) were prepared by compression molding of the respective LLDPE-dye mixtures (ES-LLDPE and EE-LLDPE), obtained by blending the components at 190 °C for 10 min in a Brabender-type mixer. The molecular dispersion of the PTCDI bis-imide derivative into LLDPE was evaluated by scanning electron microscopy (SEM) (see Supporting Information for an image of an ES-LLDPE-0.1 film, containing the highest ES-PTCDI concentration), which evidenced the absence of macro-sized aggregates of the guest molecules.

Differently from the behavior in solution, ES-PTCDI and EE-PTCDI dispersed into the LLDPE matrix showed distinguishable optical properties both in absorption and in emission. For instance, ES-LLDPE composite films displayed absorption features analogous to those reported for heptane dispersion even at low dye concentrations (0.01 wt % ES-PTCDI) showing, besides the typical absorption peaks of the isolated non-interacting chromophores at 480 and 520 nm, an unstructured band pointed at 575 nm, probably attributed to the formation of nano-/micro-sized dye aggregates (Figure 5a). On the contrary, in EE-LLDPE films, the aggregation phenomenon occurred only at higher dye concentrations (≥0.05 wt % EE-PTCDI), thus indicating a reduced packing tendency of the PTCDI bis-imide derivative functionalized by the branched alkyl chains (Figure 5b). In addition, the different absorption features of the aggregation band showed by ES-LLDPE and EE-LLDPE films in the 550−600 nm range were likely due to different supramolecular assemblies of PTCDI bis-imide dyes induced by the different alkyl functionalizations.

The emission behavior of ES-LLDPE composite films containing the 0.01 wt % ES-PTCDI derivative reflected the behavior of chloroform and diluted ($\leq 10^{-5}$ M) heptane (a medium as apolar as PE) solutions, displaying typical luminescent bands of non-interacting dyes at about 525 and 565 nm (Figure 6a). On the contrary, by increasing the ES-PTCDI concentration, the fluorescence of the ES-LLDPE films resulted in being progressively quenched at all wavelengths, thus indicating very strong $\pi-\pi$ packing among perylene chromophores. The most effective quenching effect observed for ES-PTCDI when dispersed into LLDPE probably may be attributed to a more planar chromophore conformation in the solid state with respect to solution.[37]

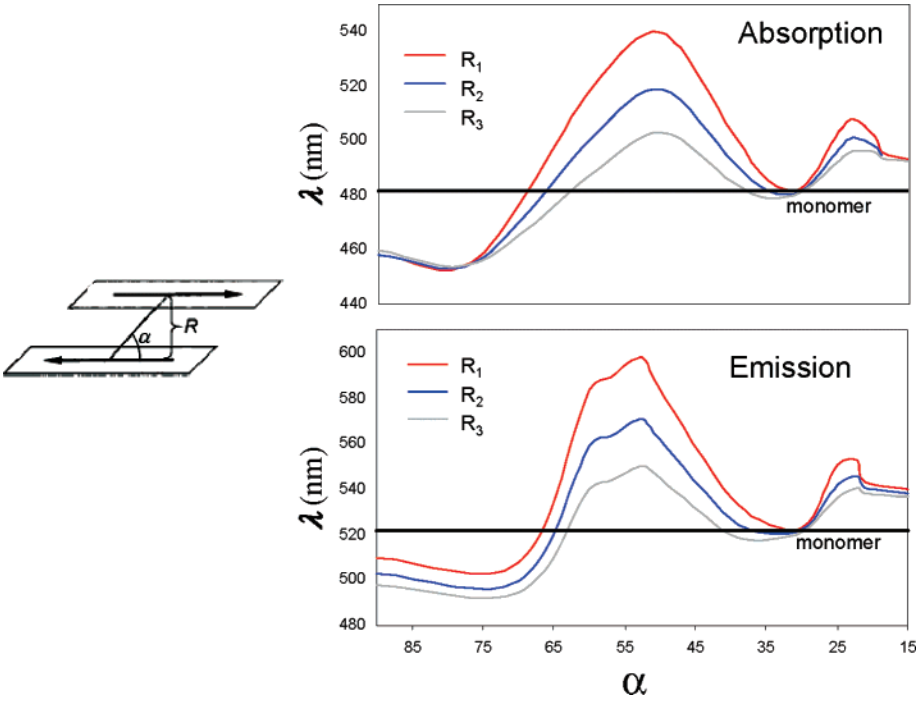

Figure 3. ZINDO absorption and emission energies (nm) of a Me-PTCDI dimer at different longitudinal shifts (i.e., different values of the tilt angle α). The three stacking values refer to $R_1 = 3.33$, $R_2 = 3.43$, and $R_3 = 3.53$ Å. The black horizontal line indicates the transition energy calculated for the monomer at the same level of QM theory.

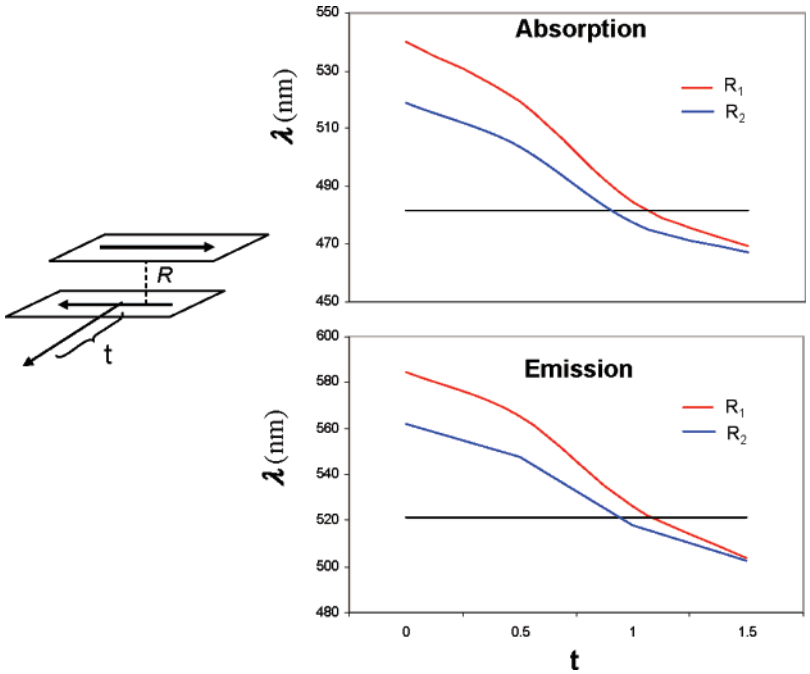

Figure 4. ZINDO absorption and emission energies (λ) of a Me-PTCDI dimer at different transversal shifts (t, in Å). The two stacking values refer to $R_1 = 3.33$ and $R_2 = 3.43$ Å, while the tilt angle is $\alpha = 50°$. The black horizontal line indicates the transition energy calculated for the monomer at the same level.

Contrary to ES-PTCDI, by increasing the EE-PTCDI concentration in LLDPE films, the emission was only partially quenched and flanked by the progressive increase of the luminescence generated by EE-PTCDI chromophoric aggregates at approximately 620 nm (Figure 6b). As analogously explained for absorption, the different behavior in emission for ES-LLDPE and EE-LLDPE films can be attributed to a dissimilar packing tendency of the two PTCDI based chromophores. The presence of branched alkyl functionalities in the EE-PTCDI dye allows the supramolecular assemblies to be slightly distorted, thus providing electronic relaxations to the ground state to be less symmetry forbidden.[29]

Analogously to the heptane solution, the alteration of the emission features of EE-LLDPE composites with dye concentration progressively turned the luminescence of EE-LLDPE films from yellow−green to red (Figure 6c).

Looking at the results reported in Figures 3 and 4, here we can try to give a more quantitative explanation of the different

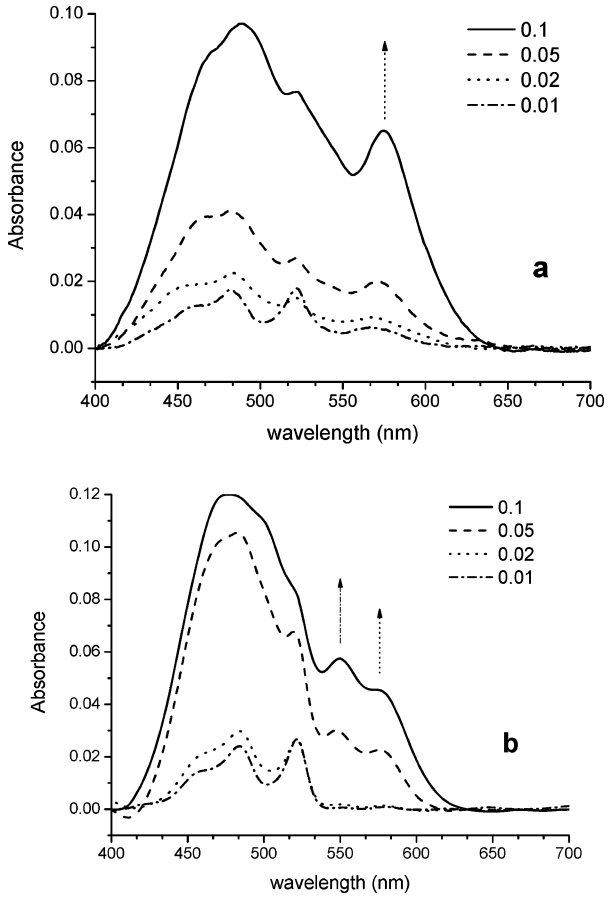

Figure 5. (a) UV−vis absorption of ES-LLDPE and (b) EE-LLDPE films at different dye concentrations.

spectroscopic behavior found for linear and branched systems embedded in the polymer matrix. As stated previously, it is reasonable to assume that due to the linear groups, ES-PTCDI aggregates can be more compact than EE-PTCDI, which bears branched and thus more bulky groups. This easily can be related to the two different wavelengths of the dimer band in the absorption spectra of the two systems (575 nm in ES vs 550 nm in EE), which indicate a stronger coupling (i.e., a more compact aggregation) between the units in the linear ES-PTCDI. We also note that the absorption spectra of EE-PTCDI seems to present two distinct bands corresponding to the aggregate form: that already mentioned at 550 nm and a second one (weaker) very similar to that present in ES, namely, at 575 nm. These two bands seem to indicate two different aggregation patterns, one less compact (and thus showing a smaller red-shift of the band with respect to the monomer) and a second more compact and thus more similar to the linear ES system.

Moving to fluorescence, however, the possible relaxation of the aggregation structure due to excitation has to be taken into account. The dependence of emission energies on stacking distance and longitudinal and transversal shifts, which are reported in Figures 3 and 4, suggests that the observed quenching in the ES-PTCDI system might be due to a longitudinal shift, which makes the lowest excited state a dark one: this shift is not large, as is shown in Figure 7, in which the oscillatory strengths for the first two excited states (I and II) as a function of the longitudinal shift (or tilt angle α) are reported: in this analysis, only two stacking distances were considered, namely, $R_1 = 3.33$ and $R_2 = 3.43$ Å. For all calculations, a ZINDO description on the CIS excited-state geometry was used.

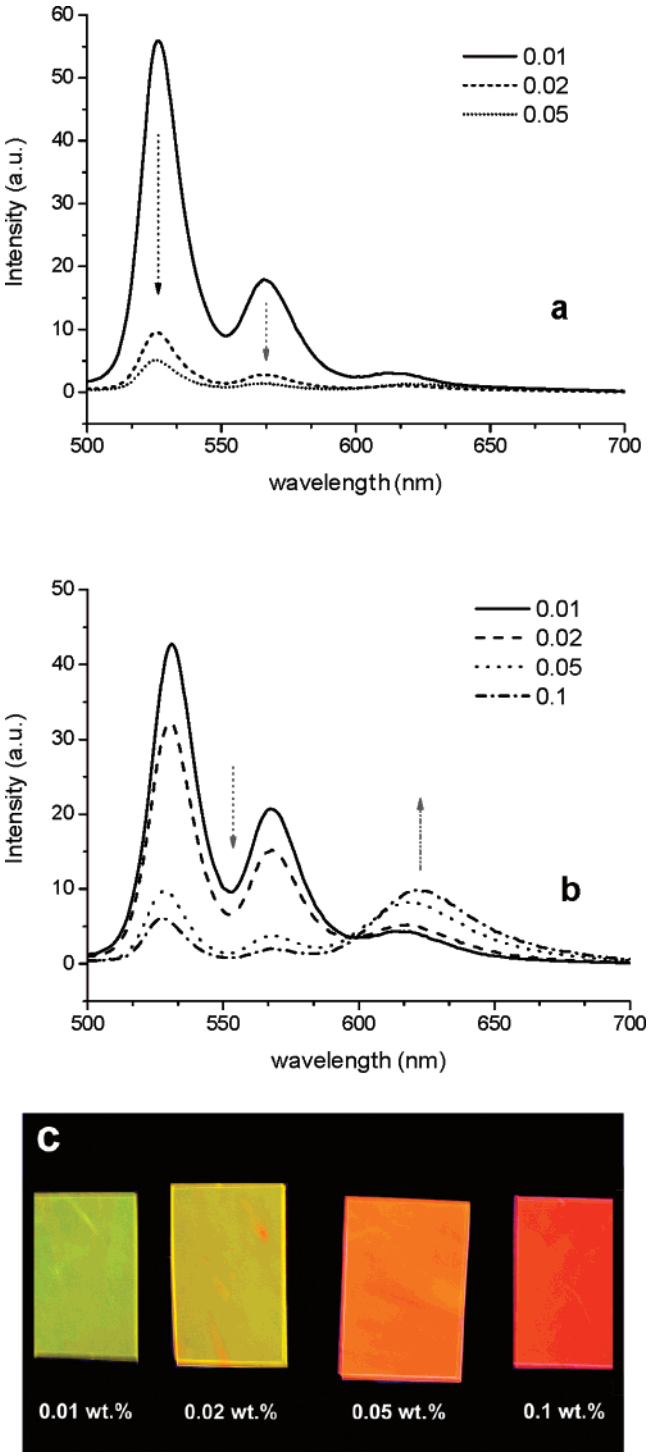

Figure 6. (a) Emission spectra of ES-LLDPE and (b) EE-LLDPE films at different dye concentrations ($\lambda_{exc} = 300$ nm). (c) Image of EE-LLDPE films taken under irradiation at 366 nm.

As it can be seen, small changes in the tilt angle around the optimum value corresponding to the dimer in the ground state (ca. 50°) lead to a drastic change in the nature of the lowest excited state (I), which becomes a dark one ($f = 0$). These relaxation effects are surely easier in the ES-PTCDI system than in the EE-PTCDI one, in which the bulky groups prevent the two monomers from being perfectly aligned along the longitudinal axes (i.e., making the tilt angle closer to 90°). By assuming that this kind of description is valid, the quenching observed in the ES system implies a relaxation of the excited state toward a more H-type aggregate (see Scheme 2), whereas

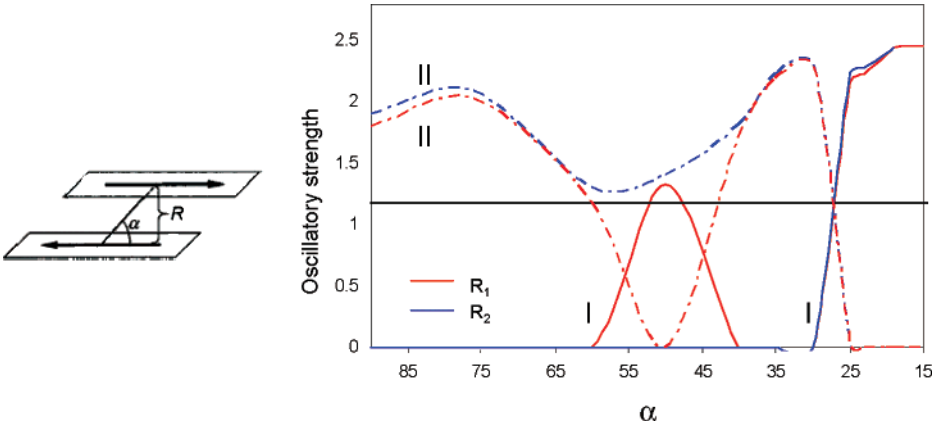

Figure 7. ZINDO oscillatory strengths of the first two excited states (I and II) for a Me-PTCDI dimer at different longitudinal shifts (i.e., different values of the tilt angle α). The two stacking values refer to $R_1 = 3.33$ and $R_2 = 3.43$ Å. The black horizontal line indicates the transition energy calculated for the monomer at the same level.

the parallel relaxation in the EE system will be much more limited due to steric hindrance of the groups; therefore, the quenching will be much less effective. This analysis remains valid if possible transverse shifts are also included.

Effect of Temperature. Because of the very high thermal transitions of perylene derivatives (melting point higher than 300 °C), the thermal stability of the dyes' supramolecular structure in LLDPE composites was only qualitatively evaluated by placing the film in contact with a hot plate at a temperature of 90 °C. In such conditions, under the excitation of a long-range UV lamp (366 nm), the red luminescence displayed by EE-PTCDI containing films and attributed to the emission of chromophoric aggregates turned progressively in less than 1 min to a brighter yellow color typical of the isolated PTCDI based chromophores. This phenomenon appeared to be reversible once the heating was stopped and faster by increasing the dye concentration (i.e., on passing from 0.05 to 0.1 wt %).

In the case of ES-LLDPE-0.02 and ES-LLDPE-0.05 films, the exposition at a temperature of 90 °C reduced the strong quenching of the luminescence, providing the films with typical emission of isolated ES-PTCDI chromophores. During heating, the different dye solubility in the polymer and the increased mobility of the macromolecular structure of PE resulted in temporarily breaking the aggregates among dyes or, likely, keeping them just at a distance at which they did not interact with each other. The results reported here were, however, limited for results obtained at 90 °C only. For a complete understanding of the phenomenon (i.e., dissolution chromophore temperature as a function of dye structure and loading), the chromophores' solubility at different regime temperatures will be investigated in the future.

Effect of Mechanical Deformation. The optical properties of the LLDPE composite films also were evaluated after applying a mechanical uniaxial deformation at room temperature or at 90 °C. It is well-established that during drawing, the macromolecular semicrystalline spherulitic structure unfolds, leading to the formation of microfibrils consisting of oriented crystalline and amorphous regions.[38] As a consequence, dye molecules dispersed in the amorphous phase of polymers[39] as isolated or interacting chromophores follow the macromolecular matrix reorganization, resulting in almost being aligned along the drawing direction.[8,12,39,40]

The uniaxial drawing of a ES-LLDPE-0.05 film (Figure 8a) promoted a strong decreasing of the dye absorption due to the fact that the composite tape became progressively thinner and

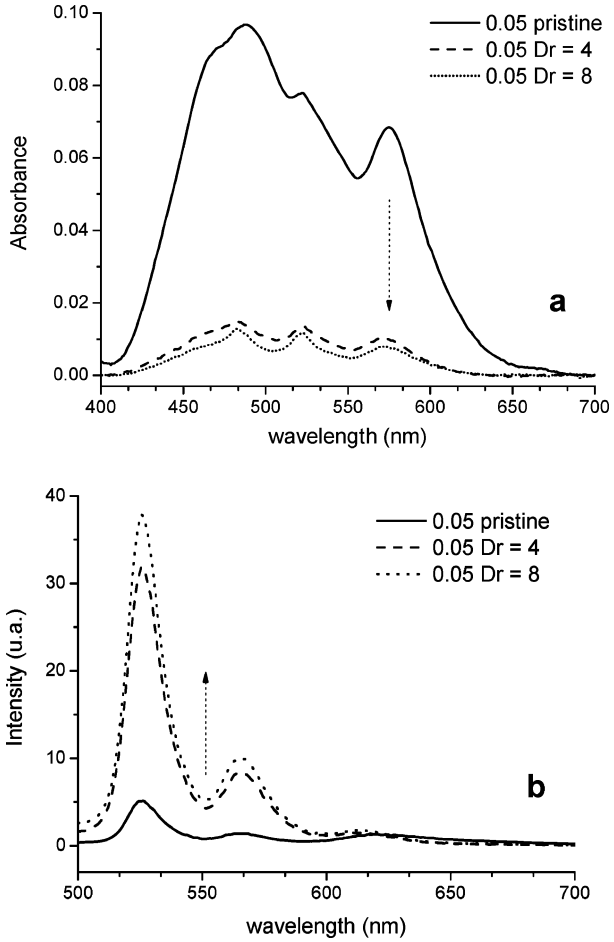

Figure 8. UV−vis absorption (a) and emission (b) ($\lambda_{exc} = 300$ nm) of a ES-LLDPE-0.05 film before and after stretching at different draw ratios (Dr = 4 and 8).

the optical density consequently was reduced (generally, the thickness of the oriented films is at least 4−5 times smaller than that of the pristine tape). The film still showed a typical absorption band of dye aggregates at about 575 nm, even at draw ratio (Dr) of 8. However, a partial disruption of ES-PTCDI aggregates occurred upon drawing as suggested by emission (Figure 8b). The ES-LLDPE-0.05 film showed a significant increase of the luminescence intensity at higher energy coming from isolated uninteracting dyes (525 nm).

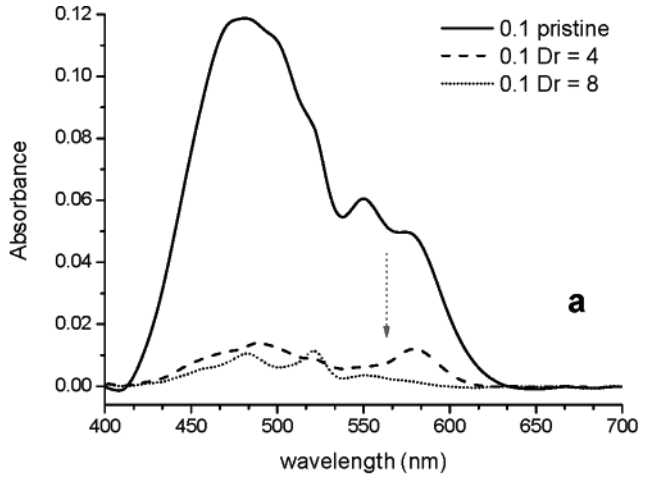

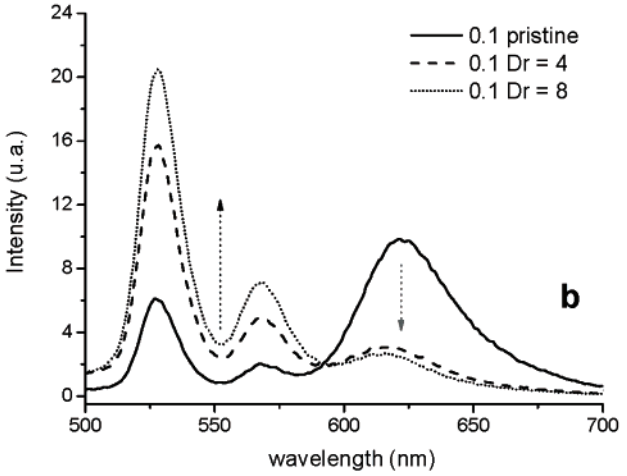

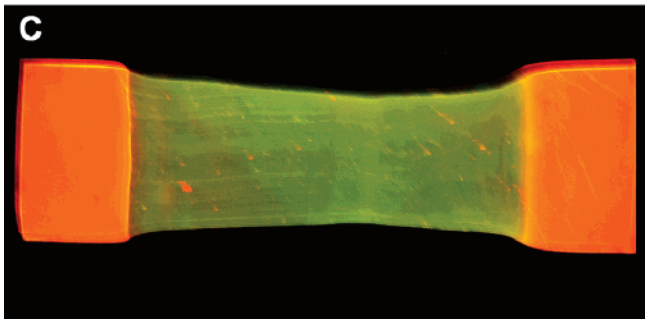

Figure 9. UV−vis absorption (a) and (b) emission (λ_{exc} = 300 nm) of a EE-LLDPE-0.1 film before and after orientation at different draw ratios (Dr = 4 and 8). (c) Digital image of the oriented film (Dr = 4) under irradiation at 366 nm.

On increasing the ES-PTCDI concentration, the effect induced by mechanical orientation on the optical features of ES-LLDPE composites was reduced due to the stronger stability of the dye aggregates.

A different optical behavior was again observed after mechanical deformation for EE-PTCDI containing LLDPE films, both in absorption and in emission. As reported in Figure 9a for a EE-LLDPE-0.1 film, the uniaxial drawing promoted two kinds of phenomena depending on the draw ratio: (a) for elongations with Dr ≤ 4, the absorption intensity decreased, and a non-negligible aggregation band at 570 nm still existed, as analogously reported for the ES-LLDPE-0.05 film; (b) on the contrary, elongations with Dr ≥ 4 were able to break up the EE-PTCDI aggregates, providing an absorption spectrum

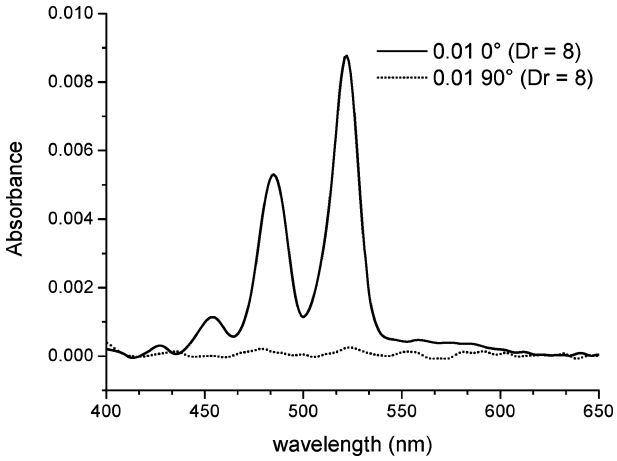

Figure 10. UV−vis absorption spectra for EE-LLBBS-0.01 oriented film (Dr = 8) as a function of the polarization angle of the incident radiation with respect to the drawing direction.

similar to that reported for EE-LLDPE composites containing low dye concentrations (≤0.05 wt %).

Once more, the effect introduced by the mechanical orientation of EE-LLDPE films was also reported in emission spectra (Figure 9b). The luminescence contribution at 625 nm, attributed to EE-PTCDI aggregates, strongly decreased at Dr = 4, whereas the fluorescence from the isolated chromophores greatly increased its intensity.

The effect of polymer matrix deformation on the emission properties also was evaluated by exposing the oriented film to a long-range UV lamp at 366 nm. The disruption of the EE-PTCDI chromophoric aggregates clearly changed the luminescence of the film from red (unoriented portion) to yellow−green (oriented portion), restoring the typical fluorescence of uninteracting PTCDI derivatives.

By reducing the EE-PTCDI concentration, the variation of the optical properties with mechanical drawing became less evident due to a lower concentration of chromophoric aggregates within LLDPE films. Once oriented, the dye doped polymeric films generally showed a dichroic behavior, especially as evidenced in the absorption whose extent depends on several factors that ranged from dye dispersibility to chromophore structure complexity.[8,9,41]

In Figure 10, the UV−vis absorption spectra of oriented EE-LLDPE-0.01 (Dr = 8) were recorded in linearly polarized light. When the polarization of the incident light was parallel to the stretching direction (0°), the film showed an absorption maximum pointed at approximately 520 nm. On the contrary, in the perpendicular configuration (90°), the absorption band resulted almost in being suppressed, thus indicating a clear anisotropic behavior of the perylene chromophores dispersed into the oriented polymer matrix. A summary of the dichroic properties in the absorption of all the oriented LLDPE films is reported in Table 3 as a function of dye concentration and drawing extent.

The best dichroic ratios as high as 19 suggested a good alignment (on average) of the perylene derivatives along the deformation direction of the polymer matrix. For all the oriented LLDPE samples, the higher the elongation, the greater the dichroic response. In addition, on passing from 0.02 to 0.1 wt % dye concentration, the dichroic ratios of the films dropped off, most likely due to the presence at high dye loading of considerable supramolecular aggregates that strongly limited the chromophore alignment. In connection with this finding, the dichroic properties of EE-LLDPE films generally appeared to be higher with respect to the ES-LLDPE oriented films. This

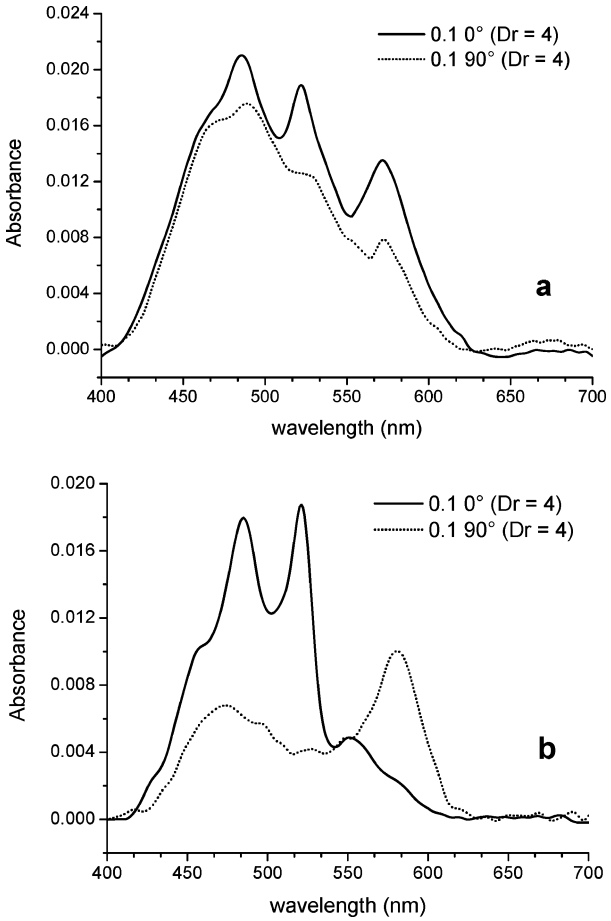

Figure 11. UV−vis absorption spectra as a function of the polarization angle for ES- LLDPE-0.1 (a) and EE-LLDPE-0.1 (b) oriented film (Dr = 4).

TABLE 3: Anisotropic Absorption Performance on Varying Chromophore Load and Draw Ratios

sample	dye	wt %	Dr	*R*
ES-LLDPE-0.01	ES-PTCDI	0.01	4	11
ES-LLDPE-0.01	ES-PTCDI	0.01	8	13
ES-LLDPE-0.02	ES-PTCDI	0.02	4	7
ES-LLDPE-0.02	ES-PTCDI	0.02	8	10
ES-LLDPE-0.1	ES-PTCDI	0.1	4	1.5
ES-LLDPE-0.1	ES-PTCDI	0.1	8	6
EE-LLDPE-0.01	EE-PTCDI	0.01	4	10
EE-LLDPE-0.01	EE-PTCDI	0.01	8	15
EE-LLDPE-0.02	EE-PTCDI	0.02	4	14
EE-LLDPE-0.02	EE-PTCDI	0.02	8	19
EE-LLDPE-0.1	EE-PTCDI	0.1	4	4.5
EE-LLDPE-0.1	EE-PTCDI	0.1	8	7

phenomenon was attributed to the presence of branched alkyl functionalities in EE-PTCDI derivatives that probably generated weaker and easily broken by mechanical drawing supramolecular aggregates with respect to the corresponding ES-PTCDI dye containing linear alkyl chains.

The dispersion degree of the PTCDI supramolecular structures therefore played a crucial role in the effectiveness of the strain effect. PTCDI derivatives dispersed in LLDPE at a concentration lower than 0.02−0.05 wt % were arranged in well-dispersed highly oriented isolated dyes or as few molecule small aggregates (down to SEM resolution, see Supporting Information), which resulted in easily being broken by mechanical drawing of the host matrix.

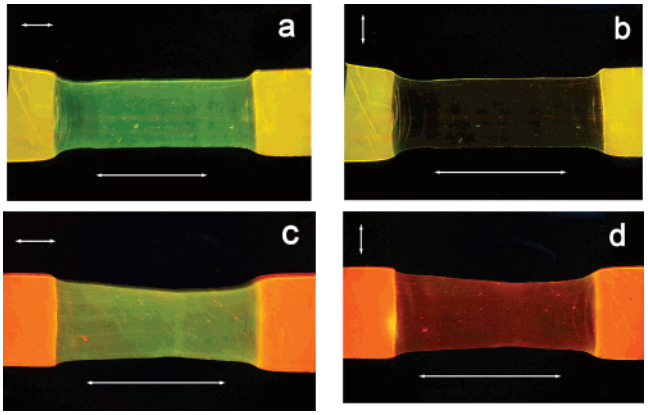

Figure 12. Digital images of oriented (Dr = 4) EE-LLDPE films containing, respectively, (a and b) 0.02 and (c and d) 0.1 wt % EE-PTCDI dye, excited at 366 nm and visualized through a polarized light parallel (a and c) and perpendicular (b and d) to the drawing direction.

On the contrary, at high dye concentrations (i.e., ≥0.05 wt %), considerable amounts of PTCDI derivatives still existed after drawing (Dr = 4) as supramolecular chromophoric assemblies limited the overall films' anisotropy but resulted interestingly in being arranged in a dichroic fashion as well. The absorption band in the range of 450−540 nm for the EE-LLDPE-0.1 film was scarcely dichroic (Dr = ∼5) according to the poor anisotropic behavior of isolated PTCDI chromophores at high concentrations. In contrast, the band at about 570 nm generated by $\pi-\pi$ stacking interactions among chromophores resulted in being suppressed by sending polarized light parallel to the stretching direction, whereas interactions emerged by rotating the linear polarizer from 0° (solid line) to 90° (short dotted curve) (Figure 11b). This result suggests that if present after polymer deformation, the electronic intermolecular interactions among PTCDI chromophores responsible for the aggregation band were mostly oriented perpendicular to the polymer uniaxial deformation. In other words, if supramolecular chromophoric assemblies still exist after mechanical deformation of the supporting solid matrix, these can be dragged by the macromolecular reorganization along the stretching direction.

PTCDI molecules able to follow the macromolecular rearrangement during stretching were obviously oriented parallel to the drawing direction; only the stacking interactions that were responsible for the aggregation band in chromophoric aggregates were oriented solidly in the perpendicular direction.

On the contrary, this phenomenon was absent for ES-LLDPE-0.1 oriented films (Dr = 4) as reported in Figure 11a. The absorption band at 570 nm still existed both for the parallel (0°) and for the perpendicular (90°) polarized light configuration, and the dichroism of the absorption of ES-PTCDI noninteracting chromophores resulted in being negligible. This behavior reflects the results reported in Table 3 (i.e., the ES-PTCDI derivative dispersed into PE was less orientable by mechanical drawing supramolecular aggregates with respect to the EE-PTCDI chromophores).

The effect of the EE-PTCDI derivative concentration on the anisotropic optical properties of oriented LLDPE based composites was also evaluated by exposing the films under irradiation at 366 nm and monitoring the emission intensity through a linear polarizer. At low EE-PTCDI concentrations (≤0.02 wt %), the oriented portion of a EE-LLDPE film (Dr = 4) appeared yellow−green due only to the presence of isolated well-dispersed perylene chromophores. By rotating the polarizer from the parallel configuration (Figure 12a) to the perpendicular

one (Figure 12b), a reduction of the emission intensity was merely observed due to the effective orientation of the perylene chromophore along the uniaxially oriented polymer matrix. By increasing the dye concentration, the oriented portion of a EE-LLDPE-0.1 film (Dr = 4) showed a green emission with the polarizer direction parallel to film stretching (Figure 12c). On the contrary, by rotating the polarizer configuration perpendicular to the drawing direction, the green component of the emission disappeared due to the uniaxial alignment of the non-interacting EE-PTCDI dyes, providing a weak but red luminescence due to the presence of residual chromophoric aggregates.

Conclusion

The incorporation of small amounts (from 0.01 to 0.1 wt %) of two different perylene tetracarboxylic acid bis-imides (perylene bis-imides) (i.e., ES-PTCDI and EE-PTCDI) into LLDPE provided composite films with modulable optical properties both in absorption and in emission. In particular, both perylene bis-imides were found to generate supramolecular aggregates promoted by $\pi-\pi$ intermolecular interactions between the conjugated planar structure of the dyes as shown by spectroscopic investigations on heptane solutions or dispersions into the LLDPE polymer matrix. The occurrence of this phenomenon effectively changed the emission of the dyes from yellow−green (non-interacting dyes) to red (interacting dyes).

Differently from solution, in LLDPE composite films, the more planar and less hindered ES-PTCDI molecular structure provided by linear alkyl chains induced the formation of chromophoric aggregates even at very low concentrations (0.01 wt %) and a more effective quenching of the fluorescence with respect to the more distorted one of the branched EE-PTCDI dyes. The latter did promote chromophore aggregation but at higher concentrations ($\geq$0.05 wt %), and the luminescence of the films resulted in being only partially quenched and characterized by the emersion of a typical emission band attributed to chromophoric aggregates (at 620 nm). This analysis was further confirmed by quantum-mechanical calculations of the absorption and emission spectra for dimers at different stacking distances and longitudinal and transversal shifts.

In addition, aggregates from the ES-PTCDI molecules resulted in being more resistant toward mechanical stretching and less orientable along the polymer drawing directions as demonstrated by UV−vis measurements in polarized light. On the contrary, LLDPE films containing EE-PTCDI derivatives showed an effective response against mechanical deformation. The emission of the films changed from red to yellow−green. In particular, for LLDPE composites containing the highest EE-PTCDI concentration (i.e., 0.1 wt %), the mechanical drawing was not able to completely disrupt all the intermolecular dye aggregates that, however, resulted in being arranged in a dichroic fashion.

In conclusion, the combination of polymer characteristics (thermoplastic semicrystalline structure composites), preparation procedure (melt blending), and dye tailored chemical structure allowed for control of the supramolecular organization of conjugated chromophores into the continuous matrix suggesting potential applications of the derived films as optical filters, linear polarizers, and smart and intelligent polyolefin based materials.

Acknowledgment. Prof. Francesco Ciardelli (DCCI, Pisa) is thanked for very helpful discussions. Financial support by MIUR-FIRB 2003 D.D.2186 Grant RBNE03R78E is acknowledged.

Supporting Information Available: Scanning electron micrograph of a ES-LLDPE-0.1 film containing 0.1 wt % EE-PTCDI derivative. This material is available free of charge via the Internet at http://pubs.acs.org.

References and Notes

(1) Crenshaw, B. R.; Kunzelman, J.; Sing, C. E.; Ander, C.; Weder, C. *Macromol. Chem. Phys.* **2007**, *208*, 572−580.
(2) Crenshaw, B. R.; Burnworth, M.; Khariwala, D.; Hiltner, A.; Mather, P. T.; Simha, R.; Weder, C. *Macromolecules* **2007**, *40*, 2400−2408.
(3) Crenshaw, B. R.; Weder, C. *Adv. Mater.* **2005**, *17*, 1471−1476.
(4) Crenshaw, B. R.; Weder, C. *Chem. Mater.* **2003**, *15*, 4717−4724.
(5) Lowe, C.; Weder, C. *Adv. Mater.* **2002**, *14*, 1625−1629.
(6) Pucci, A.; Ruggeri, G.; Bronco, S.; Bertoldo, M.; Cappelli, C.; Ciardelli, F. *Prog. Org. Coat.* **2007**, *58*, 105−116.
(7) Pucci, A.; Di Cuia, F.; Signori, F.; Ruggeri, G. *J. Mater. Chem.* **2007**, *17*, 783−790.
(8) Pucci, A.; Cappelli, C.; Bronco, S.; Ruggeri, G. *J. Phys. Chem. B* **2006**, *110*, 3127−3134.
(9) Pucci, A.; Tirelli, N.; Ruggeri, G.; Ciardelli, F. *Macromol. Chem. Phys.* **2005**, *206*, 102−111.
(10) Pucci, A.; Biver, T.; Ruggeri, G.; Itzel Meza, L.; Pang, Y. *Polymer* **2005**, *46*, 11198−11205.
(11) Pucci, A.; Bertoldo, M.; Bronco, S. *Macromol. Rapid Commun.* **2005**, *26*, 1043−1048.
(12) Tirelli, N.; Cellai, S. A. C.; Pucci, A.; Regoli, L.; Ruggeri, G.; Ciardelli, F. *Macromolecules* **2001**, *34*, 2129−2137.
(13) Geissler, G.; Remy, H. *Fluorescence Dyes*; 1962.
(14) Struijk, C. W.; Sieval, A. B.; Dakhorst, J. E. J.; van Dijk, M.; Kimkes, P.; Koehorst, R. B. M.; Donker, H.; Schaafsma, T. J.; Picken, S. J.; van de Craats, A. M.; Warman, J. M.; Zuilhof, H.; Sudholter, E. J. R. *J. Am. Chem. Soc.* **2000**, *122*, 11057−11066.
(15) Würthner, F. *Chem. Commun. (Cambridge, U.K.)* **2004**, 1564−1579.
(16) Langhals, H. *Heterocycles* **1995**, *40*, 477−500.
(17) Malenfant, P. R. L.; Dimitrakopoulos, C. D.; Gelorme, J. D.; Kosbar, L. L.; Graham, T. O.; Curioni, A.; Andreoni, W. *Appl. Phys. Lett.* **2002**, *80*, 2517−2519.
(18) Schmidt-Mende, L.; Fechtenkotter, A.; Mullen, K.; Moons, E.; Friend, R. H.; MacKenzie, J. D. *Science (Washington, DC, U.S.)* **2001**, *293*, 1119−1122.
(19) Tang, C. W. *Appl. Phys. Lett.* **1986**, *48*, 183−185.
(20) Woehrle, D.; Meissner, D. *Adv. Mater.* **1991**, *3*, 129−138.
(21) Langhals, H.; Saulich, S. *Chem.—Eur. J.* **2002**, *8*, 5630−5643.
(22) Langhals, H.; Kirner, S. *Eur. J. Org. Chem.* **2000**, *2*, 365−380.
(23) Becke, A. *J. Chem. Phys.* **1993**, *98*, 5648−5652.
(24) Lee, C.; Yang, W. *Phys. Rev. B: Condens. Matter Mater. Phys.* **1988**, *37*, 785−789.
(25) Tomasi, J.; Mennucci, B.; Cammi, R. *Chem. Rev.* **2005**, *105*, 2999−3093.
(26) Frisch, M. J.; Trucks, G. W.; Schlegel, H. B.; Scuseria, G. E.; Robb, M. A.; Cheeseman, J. R.; Montgomery, J. A., Jr.; Vreven, T.; Kudin, K. N.; Burant, J. C.; Millam, J. M.; Iyengar, S. S.; Tomasi, J.; Barone, V.; Mennucci, B.; Cossi, M.; Scalmani, G.; Rega, N.; Petersson, G. A.; Nakatsuji, H.; Hada, M.; Ehara, M.; Toyota, K.; Fukuda, R.; Hasegawa, J.; Ishida, M.; Nakajima, T.; Honda, Y.; Kitao, O.; Nakai, H.; Klene, M.; Li, X.; Knox, J. E.; Hratchian, H. P.; Cross, J. B.; Bakken, V.; Adamo, C.; Jaramillo, J.; Gomperts, R.; Stratmann, R. E.; Yazyev, O.; Austin, A. J.; Cammi, R.; Pomelli, C.; Ochterski, J. W.; Ayala, P. Y.; Morokuma, K.; Voth, G. A.; Salvador, P.; Dannenberg, J. J.; Zakrzewski, V. G.; Dapprich, S.; Daniels, A. D.; Strain, M. C.; Farkas, O.; Malick, D. K.; Rabuck, A. D.; Raghavachari, K.; Foresman, J. B.; Ortiz, J. V.; Cui, Q.; Baboul, A. G.; Clifford, S.; Cioslowski, J.; Stefanov, B. B.; Liu, G.; Liashenko, A.; Piskorz, P.; Komaromi, I.; Martin, R. L.; Fox, D. J.; Keith, T.; Al-Laham, M. A.; Peng, C. Y.; Nanayakkara, A.; Challacombe, M.; Gill, P. M. W.; Johnson, B.; Chen, W.; Wong, M. W.; Gonzalez, C.; Pople, J. A. *Gaussian 03, revision C.02*; Gaussian, Inc.: Pittsburgh, PA, 2004.
(27) Pucci, A.; Moretto, L.; Ruggeri, G. *Polymers* **2002**, *15*.
(28) Langhals, H.; Demmig, S.; Huber, H. *Spectrochim. Acta, Part A* **1988**, *44*, 1189−1193.
(29) Balakrishnan, K.; Datar, A.; Naddo, T.; Huang, J.; Oitker, R.; Yen, M.; Zhao, J.; Zang, L. *J. Am. Chem. Soc.* **2006**, *128*, 7390−7398.
(30) Bauer, P.; Wietasch, H.; Lindner, S. M.; Thelakkat, M. *Chem. Mater.* **2007**, *19*, 88−94.
(31) Würthner, F.; Thalacker, C.; Diele, S.; Tschierske, C. *Chem.—Eur. J.* **2001**, *7*, 2245−2253.
(32) Graser, F.; Haedicke, E. *Liebigs Ann. Chem.* **1984**, *3*, 483−494.
(33) Graser, F.; Haedicke, E. *Liebigs Ann. Chem.* **1980**, *12*, 1994−2011.

(34) Hädicke, E.; Graser, F. *Acta Crystallogr., Sect. C: Cryst. Struct. Commun.* **1986**, *42*, 189−195.
(35) Hädicke, E.; Graser, F. *Acta Crystallogr., Sect. C: Cryst. Struct. Commun.* **1986**, *42*, 195−198.
(36) Klebe, G.; Graser, F.; Hädicke, E.; Berndt, J. *Acta Crystallogr., Sect. B: Struct. Sci.* **1989**, *45*, 69−77.
(37) Bunz, U. H. F. *Chem. Rev.* **2000**, *100*, 1605.
(38) Ward, I. M. *Structure and Properties of Oriented Polymers*; Applied Science Publishers Ltd.: London, 1975.
(39) Phillips, P. J. *Chem. Rev.* **1990**, *90*, 425−436.
(40) Palmans, A. R. A.; Montali, M. E., A.; Weder, C.; Smith, P. *Chem. Mater.* **2000**, *12*, 472−480.
(41) Ciardelli, F.; Cellai, C.; Pucci, A.; Regoli, L.; Ruggeri, G.; Tirelli, N.; Cardelli, C. *Polym. Adv. Technol.* **2001**, *12*, 223−230.